



Since January 2020 Elsevier has created a COVID-19 resource centre with free information in English and Mandarin on the novel coronavirus COVID-19. The COVID-19 resource centre is hosted on Elsevier Connect, the company's public news and information website.

Elsevier hereby grants permission to make all its COVID-19-related research that is available on the COVID-19 resource centre - including this research content - immediately available in PubMed Central and other publicly funded repositories, such as the WHO COVID database with rights for unrestricted research re-use and analyses in any form or by any means with acknowledgement of the original source. These permissions are granted for free by Elsevier for as long as the COVID-19 resource centre remains active.



Asymptomatic COVID-19 CT image denoising method based on wavelet transform combined with improved PSO

Guowei Wang^{a,1}, Shuli Guo^{a,1}, Lina Han^{b,*}, Anil Baris Cekderi^a, Xiaowei Song^a, Zhilei Zhao^a

^a State Key Laboratory of Intelligent Control and Decision of Complex Systems, School of Automation, Beijing Institute of Technology, Beijing 100081, China

^b Department of Cardiology, The Second Medical Center, National Clinical Research Center for Geriatric Diseases, Chinese PLA General Hospital, Beijing, China

ARTICLE INFO

Keywords:

Wavelet transform
Asymptomatic COVID-19
Threshold function
Particle swarm optimization (PSO)
Gaussian noise

ABSTRACT

The quality of asymptomatic corona virus disease 2019 (COVID-19) computed tomography (CT) image is reduced due to interference from Gaussian noise, which affects the subsequent image processing. Aiming at the problem that asymptomatic COVID-19 CT image often have small flake ground-glass shadow in the early lesions, and the density is low, which is easily confused with noise. A denoising method of wavelet transform with shrinkage factor is proposed. The threshold decreases with the increase of decomposition scale, and it reduces the misjudgment of signal points. In the advanced stage, the range of lesions increases, with consolidation and fibrosis in different sizes, which have similar gray value to the CT images of suspected cases. Aiming at the problems of low contrast and fuzzy boundary in the traditional wavelet transform, the threshold function based on the optimization of parameters combined with the improved particle swarm optimization (PSO) is proposed, so that the parameters of wavelet threshold function can change adaptively according to the lung lobe and ground-glass lesions with fewer iterations. The simulation results show that the paper method is significantly better than other algorithms in peak signal-to-noise ratio (PSNR), signal-to-noise ratio (SNR) and mean absolute error (MSE). For example, aiming at the early asymptomatic COVID-19, compared with the comparison methods, the PSNR under the proposed method has increased by about 5 dB, the MSE has been greatly reduced, and the SNR has increased by about 6.1 dB. It can be seen that the denoising effect under the proposed method is the best.

1. Introduction

1.1. Background & problem domain

COVID-19 is a new type of virus that is extremely contagious, and the population lacks immunity [1]. According to reports [2], asymptomatic COVID-19 accounts for 12% of the confirmed cases. Goh [3] finds that the viral load in asymptomatic COVID-19 patients is similar to that in symptomatic patients, suggesting that asymptomatic patients have the potential to spread the virus. This paper intends to analyze asymptomatic COVID-19 CT image denoising, so as to reduce the rate of missed and mistake diagnosis for asymptomatic COVID-19 patients. It is helpful for the subsequent image processing and doctors' judgment of patients' condition.

1.2. Review of literature

CT images will produce high-dose radiation in the process of acquisition, which will pose a great threat to the patient's health. The damage to the patient's body is usually reduced by decreasing the CT dose at present. But CT images taken with low dose usually have Gaussian noise. In addition, when the dose remained constant, the fatter the subject, the greater the noise. Relevant experiments have proved that when the volume of the subject increases by 8 cm, the Gaussian noise will double. On the other hand, the medical equipment is used for a long time and the use environment is poor, resulting in poor heat dissipation, which will also produce Gaussian noise. The asymptomatic COVID-19 CT image will inevitably be polluted by Gaussian noise during transmission, which causes the image to be blurred and affects the quality of the subsequent processing. Therefore, an effective image denoising method is very important. Wavelet transform can adjust the sampling length of different frequencies in time domain, and it has the characteristic of multi-

* Corresponding author.

E-mail address: 2438381279@qq.com (L. Han).

¹ These authors contributed equally to this work.

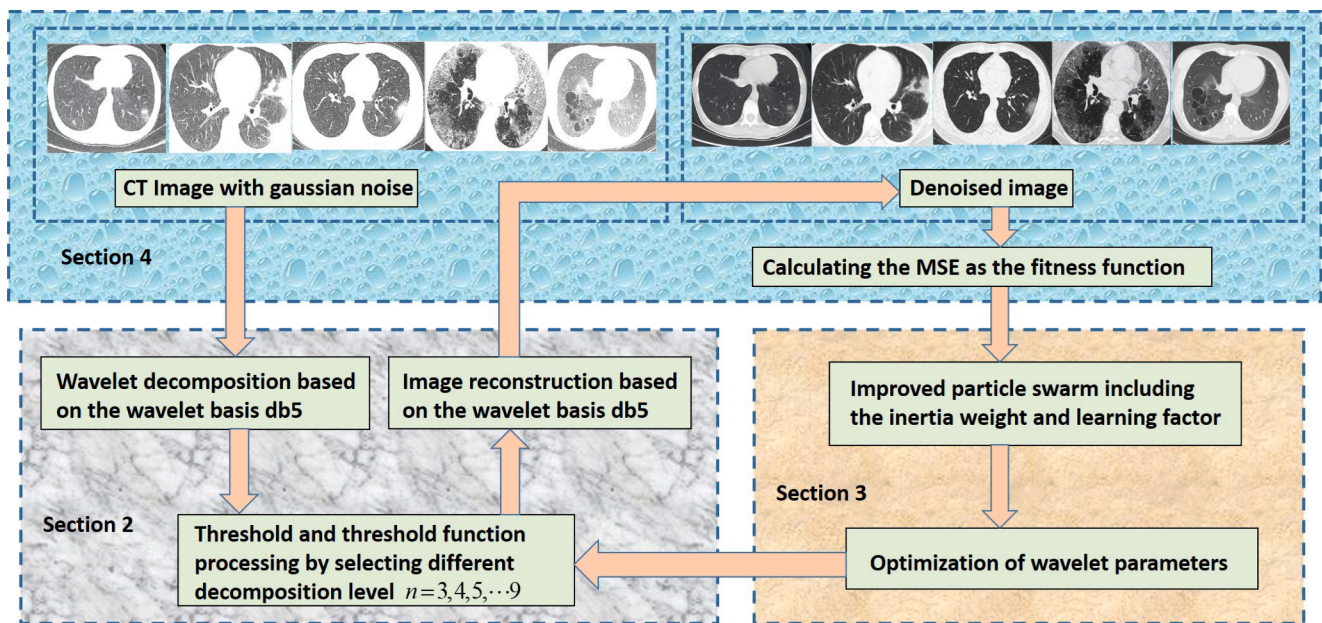


Fig. 1. Paper structure.

resolution for Gaussian noise [4,5]. However, the traditional wavelet transform has some problems of constant deviation and discontinuous threshold. Hence, some scholars have researched on it. Reference [6] proposed a new threshold function, which has an adjustment factor. Although the threshold function can be adjusted dynamically, the denoising effect is not very ideal. Reference [7] proposed to add the adjustment parameters to optimize the typical hard and soft threshold, but the effect has been improved to a certain extent. Reference [8] proposed wavelet transform based on multi-layer threshold function, which adjusts the threshold factor according to the different sampling length, but it did not analyze the influence on the denoising effect. Reference [9] proposed an adaptive threshold function, which reduces the deviation between the original wavelet coefficients and the estimated wavelet coefficients by setting appropriate adjustment parameters, but the denoising effect is not ideal. Reference [10] proposed an improved wavelet threshold with symbolic function, and it set different adjustment factors to compare and analyze the changes of PSNR. It can be seen from the simulation results that there is still a constant deviation. Reference [11] proposed a new threshold function combined with the traditional hard and soft threshold. Through the comparison of simulation results, it can be seen that the PSNR increases, but the effect is not particularly significant. Reference [12] made full use of 3D wavelets and proposed a weighted 3D wavelet denoising algorithm based on the principle of volume sub-band weighting. The sub-band weighting aims to better improve the image representation ability and adaptively remove noise in the image, and it has a good noise coefficient representation ability. Reference [13] proposed the framework of dual tree complex wavelet transform (DTCWT). DTCWT overcomes the defects of wavelet transform. It also has translation invariance and multi-directional selectivity, which can express the characteristics of image more effectively. Reference [14] proposed an image denoising method in the dual-tree complex wavelet transform domain, which combines multi-level median filtering in the complex wavelet domain to remove the noise caused by the imaging environment and imaging firmware defects. Reference [15] proposed to introduce the bivariate statistical model into the real part and the imaginary part coefficients of dual tree complex wavelet transform, and the joint probability model of real part and imaginary part coefficients was used as the mathematical model to remove Gaussian noise. Reference [16] combined the unsampled wavelet transform with the dual-tree complex wavelet transform to

produce an unsampled dual-tree complex wavelet transform, which provides improved low-scale sub-band localization and improved direction selectivity for better Gaussian noise removal. Reference [17] proposed a dual-tree complex wavelet transform which combines singular value decomposition and Frobenius energy correction factor, and the image is threshold processed with a binary shrink function (SVDBL). However, the Frobenius energy correction factor lacks theoretical basis, which is difficult to apply to different images and it has poor robustness. Reference [18] improved the DTCWT filter and proposed the integer DTCWT filter, which reduces the hardware complexity of the method and it has the advantages of DTCWT translation invariance and multi-directional selectivity. However, its disadvantage is that it reduces the representation accuracy of the image coefficients and ignores the subtle features of the image.

1.3. Gaps identified from review

The above improved algorithms have great improvements in denoising performance, which reduce the deviation between the original wavelet coefficients and the estimated wavelet coefficients, so as to improve the approximation between the reconstructed image and the original image to a certain extent, but there are still some deficiencies in dealing with image detail blur. Asymptomatic COVID-19 CT image shows small pieces of ground-glass shadow in the early lesions, and its border has halo sign, which is easily confused by noise. On the other hand, the lesions of asymptomatic COVID-19 show uneven in the advanced stage, which is similar to the CT image of suspected cases such as influenza virus and staphylococcal pneumonia. The traditional wavelet transform has problems of low contrast and fuzzy boundary.

1.4. Paper structure

The rest of this paper is organized as follows. Section 2 describes the wavelet transform including the wavelet threshold and the threshold function. We present its mathematical properties. In Section 3, we propose the improved particle swarm including the inertia weight and learning factor for optimization of wavelet parameters. In Section 4, we show the simulation experiments for the different kinds of CT images including early asymptomatic COVID-19, advanced asymptomatic COVID-19, resolution asymptomatic COVID-19, influenza virus

(suspected case of asymptomatic COVID-19), staphylococcal pneumonia (suspected case of asymptomatic COVID-19). This paper is structured as shown in Fig.1.

1.5. Highlights

The objective of this paper is to denoise the asymptomatic COVID-19 CT images better, which is helpful for the subsequent image processing and doctors' judgment of patients' condition. The highlights of this work can be summarized as the following: (i) In Section 2, an improved wavelet threshold based on the shrinkage factor is proposed. In this method, the threshold decreases with the increase of decomposition scale. It improves the accuracy of noise detection to a greater extent for asymptomatic COVID-19; (ii) In Section 2, we develop the wavelet threshold function based on the adjustment factor integrated with the arc tangent, which overcomes the discontinuity and the constant deviation of the traditional threshold function. It is suitable for noisy signals with different variance; (iii) In Section 3, a wavelet transform based on the optimization of parameters combined with improved PSO is proposed, so that the wavelet parameters can change adaptively according to the details of lung lobes and ground-glass shadow with relatively few iterations; (iv) In Section 4, aiming at the different kinds of asymptomatic COVID-19 CT images, the simulation experiments prove that the paper method has strong robustness to Gaussian noise, which enhances the ability of image denoising while better protecting the details of the lesion. It reduces the rate of missed and mistake diagnosis for asymptomatic COVID-19.

2. Principle and calculation of wavelet transform denoising

2.1. Principle of wavelet transform

An image model $f(j,l)$ containing Gaussian noise [19] is expressed as:

$$f(j,l) = g(j,l) + n(j,l) \quad (1)$$

Where, $f(j,l)$ represents the image with Gaussian noise; $g(j,l)$ represents the original image without noise; $n(j,l)$ represents Gaussian noise and it follows normal distribution $N(0, \delta^2)$; (j,l) represents the pixel position of the image. The main steps of wavelet transform denoising are as follows: a) The wavelet coefficient $w_{j,l}$ is obtained by wavelet transforming of $f(j,l)$; b) The threshold of each decomposition scale is set, and the wavelet coefficient $w_{j,l}$ is processed by the threshold function to obtain the wavelet estimation coefficient $\hat{w}_{j,l}$; c) The wavelet estimation coefficients are used to reconstruct the denoised image $\hat{f}_{j,l}$.

2.2. Calculation of wavelet threshold

The calculation of threshold directly affects the denoising effect. At present, the traditional threshold calculation methods include Stein unbiased likelihood estimation [20], heuristic threshold [21], maximum and minimum threshold [22], fixed threshold [23]. Aiming at the problems that the image detail is easy to be lost and the denoising effect is not obvious in the traditional threshold. This paper proposes an improved wavelet threshold based on the shrinkage factor, which is expressed as:

$$\lambda = \frac{\delta \sqrt{2 \ln(M \times N) \times e^{1/n}}}{\ln(n+1)} \times z \quad (2)$$

Where, $\frac{\sqrt{e^{1/n}}}{\ln(n+1)}$ is the shrinkage factor. n is the number of decomposition scale. $M \times N$ represents the size of the image. δ represents the variance of Gaussian noise, and the expression is $\delta = \frac{\text{median}(|w_{j,l}|)}{0.6745}$. The wavelet threshold will gradually decrease with the increase of decomposition scale, which has good adaptability and better denoising effect. z is an

adjustable parameter.

2.3. Improvement of wavelet threshold function

The traditional hard threshold function [24] has the problem that the continuity of wavelet estimation coefficients is very poor, which is discontinuous at $\pm\lambda$. Therefore, the reconstructed image will produce oscillation and truncation effect. The soft threshold function has good continuity, but there is a certain deviation between the wavelet coefficients and the estimated coefficients, thus the final denoising effect is not very ideal. This paper improves the threshold function by increasing the adjustment factor integrated with the arc tangent to reduce the constant deviation between the original wavelet coefficients and the estimated coefficients, and its expression is:

$$\hat{w}_{j,l} = \begin{cases} (1-\mu)w_{j,l} + \mu \text{sgn}(w_{j,l}) \left(|w_{j,l}| - m \times \lambda e^{\arctan(|w_{j,l}|-\lambda)^a} \right), & |w_{j,l}| \geq \lambda \\ \text{sgn}(w_{j,l}) \left[w_{j,l}^{2t+1} \left(e^t - 1/2 \right) \lambda^{-2t} \right], & |w_{j,l}| < \lambda \end{cases} \quad (3)$$

Where, $u = e^{-b(|w_{j,l}|-\lambda)^2}$; a, b, m and t are adjustable parameters, and they are all positive numbers, so the denoising performance of the threshold function can be improved by selecting different value of parameters. Moreover, in the interval of $|w_{j,l}| < \lambda$, the threshold function is not directly set to 0, it is gradually compressed through a nonlinear function, which can avoid the oscillation effect caused by the direct truncation of the traditional threshold function. From the view of mathematical point to examine the improved threshold function: 1) Analysis of function continuity

$$\begin{aligned} \lim_{w_{j,l} \rightarrow \lambda^+} \hat{w}_{j,l} &= \lim_{w_{j,l} \rightarrow \lambda^+} \left[(1-\mu)w_{j,l} + \mu \text{sgn}(w_{j,l}) \left(|w_{j,l}| - m \times \lambda e^{\arctan(|w_{j,l}|-\lambda)^a} \right) \right] = \\ \lim_{w_{j,l} \rightarrow \lambda^+} \left[\mu \text{sgn}(w_{j,l}) \left(|w_{j,l}| - m \times \lambda e^{\arctan(|w_{j,l}|-\lambda)^a} \right) \right] &= \\ \lim_{w_{j,l} \rightarrow \lambda^+} \left[\text{sgn}(w_{j,l}) \left(|w_{j,l}| - m \times \lambda e^{\arctan(|w_{j,l}|-\lambda)^a} \right) \right] &= \\ \lim_{w_{j,l} \rightarrow \lambda^+} \left[w_{j,l} - m \times \lambda e^{\arctan(|w_{j,l}|-\lambda)^a} \right] &= 0 \end{aligned} \quad (4)$$

Where, $\lim_{w_{j,l} \rightarrow \lambda^+} \hat{w}_{j,l} = 0$, $\lim_{w_{j,l} \rightarrow \lambda^-} \hat{w}_{j,l} = 0$. Then there is $\lim_{w_{j,l} \rightarrow \lambda^+} \hat{w}_{j,l} = \lim_{w_{j,l} \rightarrow \lambda^-} \hat{w}_{j,l} = 0$, indicating that the threshold function is continuous at λ .

$$\begin{aligned} \lim_{w_{j,l} \rightarrow -\lambda^-} \hat{w}_{j,l} &= \lim_{w_{j,l} \rightarrow -\lambda^-} \left[(1-\mu)w_{j,l} + \mu \text{sgn}(w_{j,l}) \left(|w_{j,l}| - m \times \lambda e^{\arctan(|w_{j,l}|-\lambda)^a} \right) \right] = \\ \lim_{w_{j,l} \rightarrow -\lambda^-} \left[-\mu \left(|w_{j,l}| - m \times \lambda e^{\arctan(|w_{j,l}|-\lambda)^a} \right) \right] &= \\ \lim_{w_{j,l} \rightarrow -\lambda^-} \left[- \left(|w_{j,l}| - m \times \lambda e^{\arctan(|w_{j,l}|-\lambda)^a} \right) \right] &= \\ \lim_{w_{j,l} \rightarrow -\lambda^-} \left(\lambda - m \times \lambda e^{\arctan(|w_{j,l}|-\lambda)^a} \right) &= 0 \end{aligned} \quad (5)$$

Where, $\lim_{w_{j,l} \rightarrow -\lambda^-} \hat{w}_{j,l} = 0$, $\lim_{w_{j,l} \rightarrow -\lambda^+} \hat{w}_{j,l} = 0$. Then there is $\lim_{w_{j,l} \rightarrow -\lambda^-} \hat{w}_{j,l} = \lim_{w_{j,l} \rightarrow -\lambda^+} \hat{w}_{j,l} = 0$, indicating that the threshold function is also continuous at $-\lambda$. In conclusion, the improved threshold function is continuous at $\pm\lambda$. 2) Analysis of function deviation

$$\begin{aligned} \lim_{w_{j,l} \rightarrow +\infty} (\hat{w}_{j,l} - w_{j,l}) &= \lim_{w_{j,l} \rightarrow +\infty} \left[(1-\mu)w_{j,l} + \mu \text{sgn}(w_{j,l}) \left(|w_{j,l}| - m \times \lambda e^{\arctan(|w_{j,l}|-\lambda)^a} \right) - w_{j,l} \right] = \\ \lim_{w_{j,l} \rightarrow +\infty} (w_{j,l} - w_{j,l}) &= 0 \end{aligned} \quad (6)$$

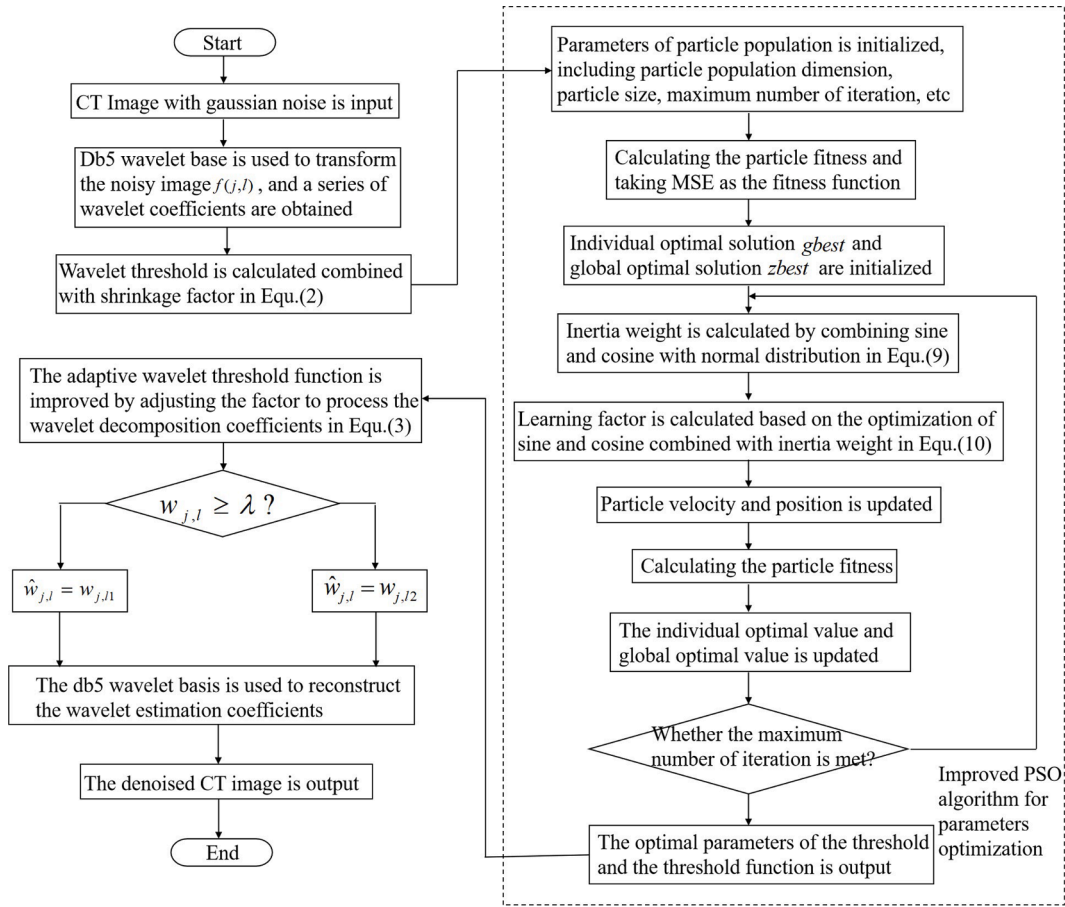


Fig. 2. Flow chart of wavelet transform combined with improved PSO.

$$\lim_{w_{j,l} \rightarrow -\infty} (\hat{w}_{j,l} - w_{j,l}) = \lim_{w_{j,l} \rightarrow -\infty} \left[(1 - \mu) w_{j,l} + \mu \operatorname{sgn}(w_{j,l}) (|w_{j,l}| - m \times \lambda e^{\arctan(|w_{j,l}| - \lambda)^a}) - w_{j,l} \right] = 0 \quad (7)$$

$$\lim_{w_{j,l} \rightarrow -\infty} (w_{j,l} - w_{j,l}) = 0$$

Therefore, $\lim_{w_{j,l} \rightarrow +\infty} (\hat{w}_{j,l} - w_{j,l}) = \lim_{w_{j,l} \rightarrow -\infty} (\hat{w}_{j,l} - w_{j,l}) = 0$ can be obtained. When increases, the deviation between and will gradually decreases, which can overcome the problem of constant deviation in the soft threshold function. 3) Influence analysis of threshold adjustable factors a, b, m and t When $|w_{j,l}| \geq \lambda$, a = 0 and b = 0, the improved threshold function is hard threshold function. When $b \rightarrow \infty$, the improved threshold function is soft threshold function. Therefore, the improved threshold function can be adjusted between soft and hard threshold function. In the interval of $|w_{j,l}| < \lambda$, the value of threshold can be adjusted by selecting different value of t. In summary, by analyzing the continuity, deviation and adjustable factors of the improved threshold function, it can be seen from the proof that the threshold function in this paper overcomes the discontinuity of the hard threshold function and the constant deviation of the wavelet coefficients in the soft threshold function.

3. Optimization of wavelet transform parameters based on improved PSO algorithm

3.1. Basic PSO algorithm

The parameters of a, b, m, t and z are optimized by the improving PSO algorithm. The basic formula for the velocity and position of the particle swarm [25] is:

$$\begin{cases} v_{id}^{t+1} = wv_{id}^t + c_1r_1(gbest_{id}^t - x_{id}^t) + c_2r_2(zbest_{gd}^t - x_{id}^t) \\ x_{id}^{t+1} = x_{id}^t + v_{id}^{t+1} \end{cases} \quad (8)$$

Where, $d = 1, 2, \dots, n$ (n represents the dimension of feature space); $i = 1, 2, \dots, m$ (m represents population size); t represents the current particle evolution algebra; w represents the inertia weight; c_1 and c_2 represent learning factor; r_1 and r_2 represent the random number in [0,1]; v_{id}^t represents the velocity of the particle in the feature space; x_{id}^t represents the position of the particle; $gbest_{id}^t$ represents the individual optimal solution; $zbest_{gd}^t$ represents the global optimal solution of the population.

3.2. Improvement of inertia weight

In the advanced stage of asymptomatic COVID-19, the lesion is larger than that of the early stage, with consolidation and fibrosis in different sizes. The ground-glass shadow is uneven and it have similar gray value to the CT image of suspected cases such as influenza virus and staphylococcal pneumonia. Aiming at the problems of low contrast and fuzzy boundary in the traditional denoising method, a wavelet transform combined with improved PSO is proposed. The wavelet denoising parameters can be changed adaptively according to the details of lung lobes and ground-glass shadow lesion with relatively few iterations. The inertia weight based on combining sine and cosine with normal distribution is proposed, the expression is:

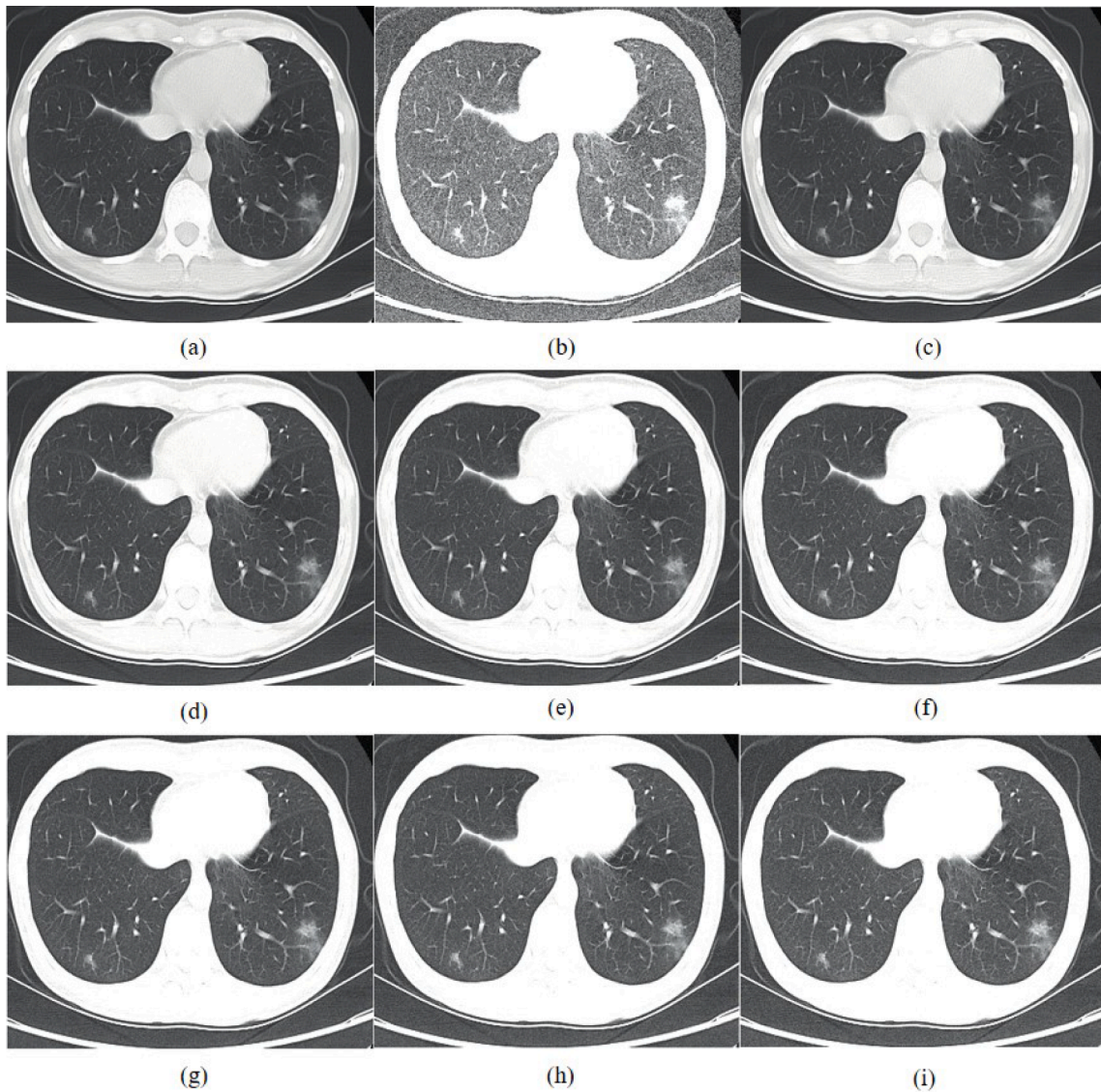


Fig. 3. CT image of early asymptomatic COVID-19: (a) impulse (30%) noise; (b) original CT image; (c) denoised image by WTPSO; (d) denoised image by BSTF; (e) denoised image by TATF; (f) denoised image by MLTF; (g) denoised image by ISTF; (h) denoised image by STF; (i) denoised image by HTF.

$$w = w_{max} \times \left(1 - \sin\left(\frac{\pi \times t}{2 \times T_{max}}\right) \right) + \frac{1}{\sqrt{2\pi}\theta} (w_{max} - w_{min}) \times \left(e^{-\frac{(t/T_{max})^k}{2\theta^2}} - e \right) \times \cos\left(\frac{\pi \times t}{2 \times T_{max}}\right) + rand \times w_{min} \times \sin\left(\frac{\pi \times t}{2 \times T_{max}}\right) \quad (9)$$

Where, w_{max} represents the maximum coefficient of inertia weight; w_{min} represents the minimum coefficient of inertia weight and t represents the current number of iteration; T_{max} represents the maximum number of iteration and k represents the nonlinear control factor; θ represents the degree of dispersion for the normal distribution, $\theta = 0.4433$; $rand$ represents a random number between (0, 1).

3.3. Improved learning factor

In the traditional PSO algorithm, the value of learning factors c_1 and c_2 is usually fixed [26], which is not set according to different stages. The learning factor based on combining sine and cosine with inertia weight is proposed, which satisfies the relationship of “as one falls,

another rises” between c_1 and c_2 , the expression is:

$$\begin{cases} c_1 = \frac{2.5 \sin\left[\frac{\pi}{2} \left(1 - \frac{t}{T_{max}}\right)\right]}{1 + e^{-w}} \\ c_2 = 2.5 - 2.5 \cos\left[\frac{\pi}{2} \left(1 + \frac{t}{T_{max}}\right)\right] \end{cases} \quad (10)$$

Where, t represents the current number of iteration and T_{max} represents the maximum number of iteration. By adjusting the learning factor, the particles are searched in a large range at the initial stage in order to obtain a variety of high-quality particles. In the later stage, they continue to learn from the global optimization and get rid of the interference of local extremum as much as possible, so as to improve the accuracy of the solution. The steps of the CT image denoising method based on the wavelet transform combined with the improved PSO algorithm are as following: a) Step 1: we select the wavelet basis function db5 and perform wavelet transform on the noisy image $f(j,l)$ to obtain a set of wavelet decomposition coefficients $w_{j,l}$; b) Step 2: the noise variance δ is calculated by $\delta = \frac{\text{median}(|w_{j,l}|)}{0.6745}$. On this basis, the threshold λ is calculated by Equ. (2). The wavelet decomposition coefficient $w_{j,l}$ is

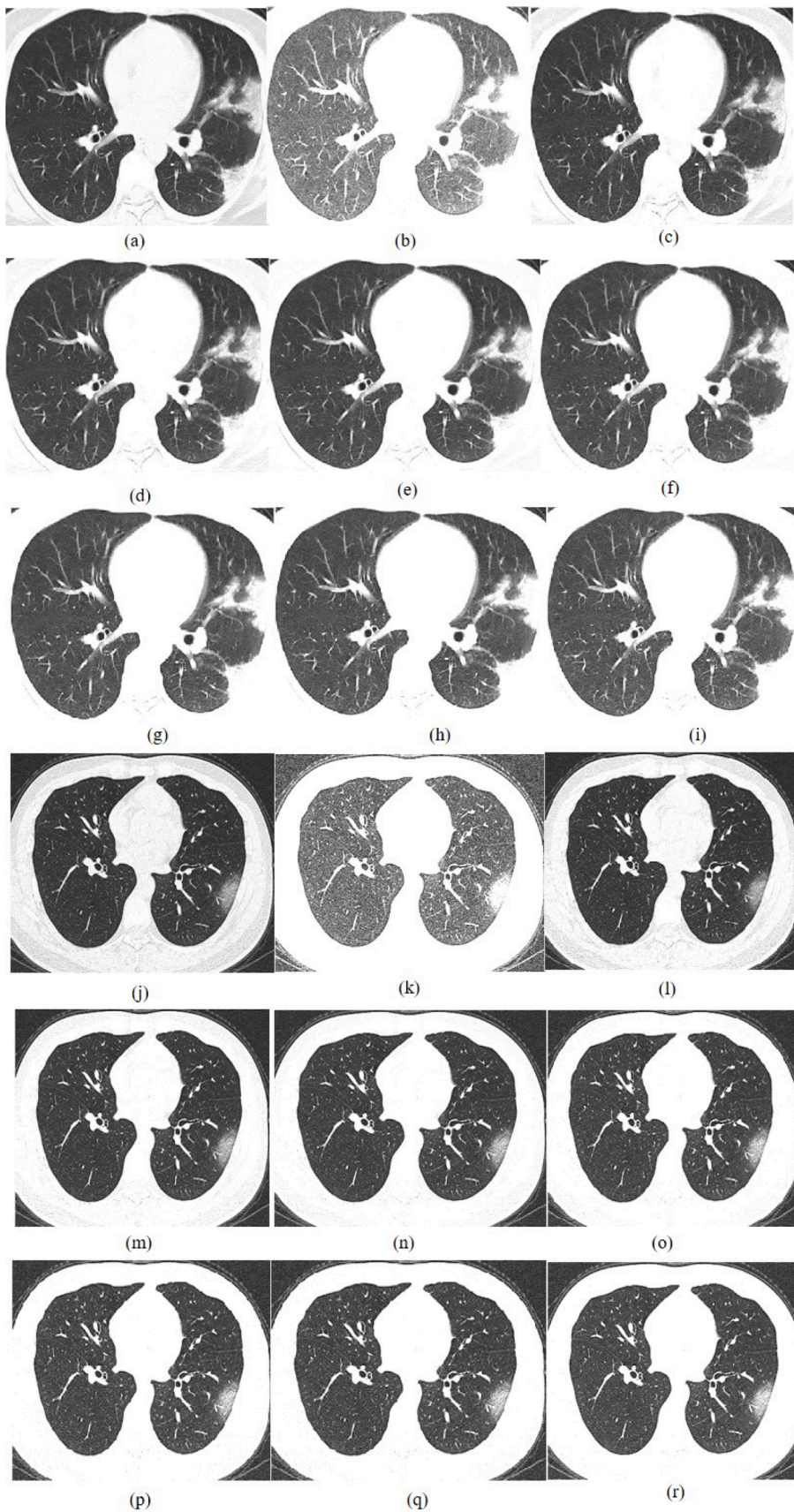


Fig. 4. CT image of advanced asymptomatic COVID-19: (a) impulse (30%) noise; (b) original CT image; (c) denoised image by WTPSO; (d) denoised image by BSTF; (e) denoised image by TATF; (f) denoised image by MLTF; (g) denoised image by ISTF; (h) denoised image by STF; (i) denoised image by HTF. CT image of resolution asymptomatic COVID-19: (j) impulse (30%) noise; (k) original CT image; (l) denoised image by WTPSO; (m) denoised image by BSTF; (n) denoised image by TATF; (o) denoised image by MLTF; (p) denoised image by ISTF; (q) denoised image by STF; (r) denoised image by HTF.

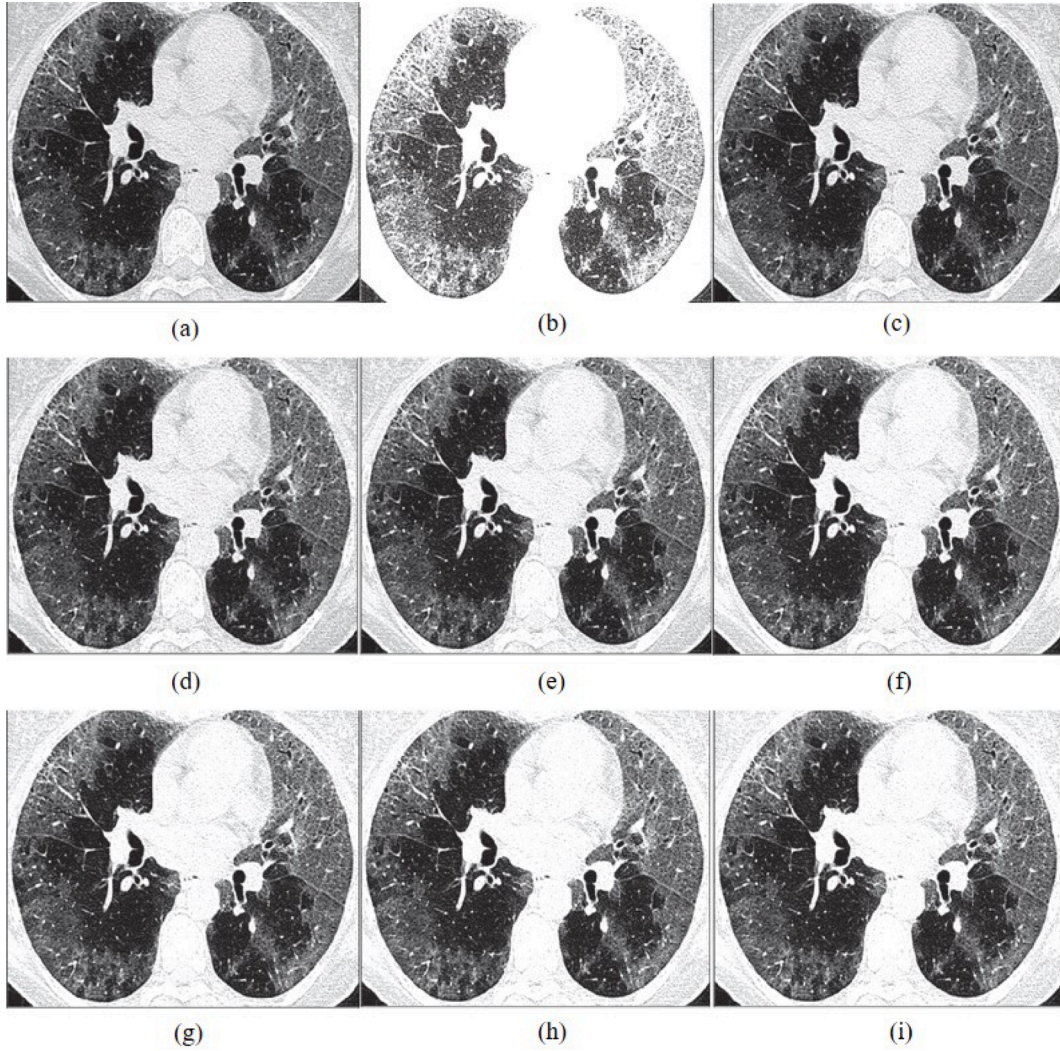


Fig. 5. CT image of influenza virus (suspected cases of COVID-19): (a) impulse (30%) noise; (b) original CT image; (c) denoised image by WT PSO; (d) denoised image by BSTF; (e) denoised image by TATF; (f) denoised image by MLTF; (g) denoised image by ISTF; (h) denoised image by STF; (i) denoised image by HTF.

processed by Equ. (3). When $|w_{j,l}| \geq \lambda$, the expression of the estimated wavelet coefficient is $\hat{w}_{j,l1} = (1 - \mu)w_{j,l} + \mu \text{sgn}(w_{j,l})(|w_{j,l}| - m \times \lambda e^{\arctan(|w_{j,l}| - \lambda)^{\alpha}})$. When $|w_{j,l}| < \lambda$, the expression of the estimated wavelet coefficient is $\hat{w}_{j,l2} = \text{sgn}(w_{j,l})[w_{j,l}^{2\alpha+1}(e^t - 1/2)\lambda^{-2t}]$; c) Step 3: the parameters of the wavelet transform is optimized by the improved PSO. The value of MSE is taken as the fitness function [27][28]. The inertia weight is calculated by Equ. (9) and the learning factor is calculated by Equ. (10). When the number of iteration is exceeded, the optimal parameters of the wavelet transform is output and then the estimated wavelet coefficient $\hat{w}_{j,l}$ is obtained. d) Step 4: the wavelet basis function db5 is used for wavelet reconstruction to obtain the denoised image $\hat{f}_{j,l}$. The flow of the improved algorithm in this paper is shown in the Fig.2. (See Fig.3)

3.4. Theoretical analysis of average computational time complexity of improved PSO

This section analyzes and compares the average computational time complexity of the improved PSO algorithm and the traditional PSO algorithm. According to the above description of the traditional PSO algorithm and the improved PSO algorithm, it can be seen that for the traditional PSO algorithm, the value of the particle inertia weight and the learning factor in each iteration remain unchanged. Assuming that the operation time required for each iteration of each particle in the i -th

step is T_i , where, $i = 1, 2, \dots, m$. m represents the maximum number of iteration, so there is $T_1 = T_2 = \dots = T_m = T$. Assuming that the number of particles in the iteration is N , it can be concluded that the total running time required by the traditional PSO algorithm for optimization is $N \times m \times T$. For the improved PSO algorithm proposed in this paper, the value of the inertia weight of the particles decreases with the number of iterations, and the learning factors are complementary. Therefore, there is $T_1 \geq T_2 \geq \dots \geq T_m$. Assuming that the number of particles in the iteration is N , the total running time required by the improved PSO optimization is $\sum_{i=1}^m N \times T_i$. It can be seen from the above analysis that the difference in the computational complexity between the improved PSO and the traditional PSO is mainly reflected in the running time required by each particle in each iteration. The following section will analyze the average computational time complexity of the algorithm based on the experimental results.

4. Experimental results and analysis

In order to verify the effectiveness of the improved threshold function, the wavelet basis function db5 is used for different layers of decomposition and reconstruction. The size of the test image is 512×512 ($M = 512, N = 512$). The software platform is Intel E8200 CPU 2.5 GHz, RAM 8G, windows 10 and MATLAB 2016a. Bayes shrink threshold function(BSTF) [4], traditional adaptive threshold function(TATF) [29],

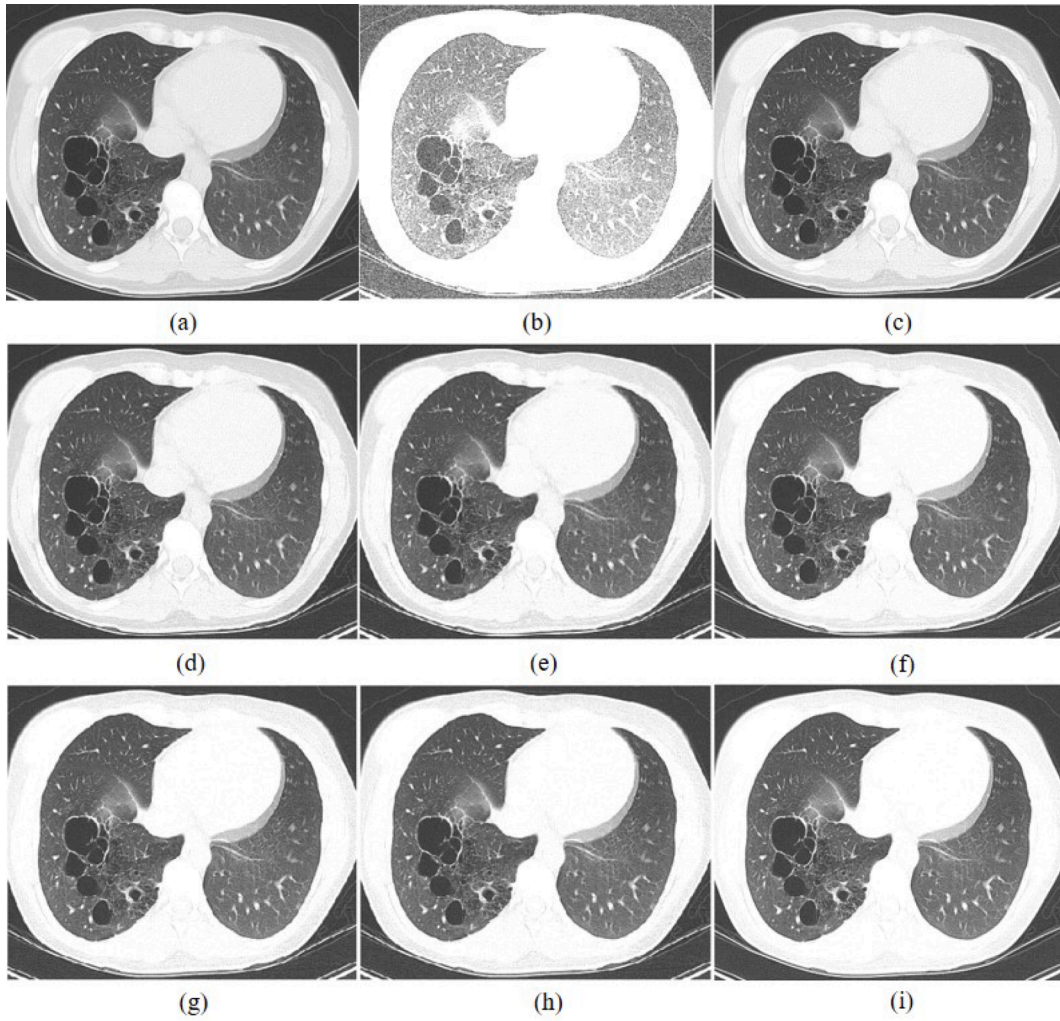


Fig. 6. CT image of staphylococcal pneumonia (suspected cases of COVID-19): (a) impulse (30%) noise; (b) original CT image; (c) denoised image by WTPSO; (d) denoised image by BSTF; (e) denoised image by TATF; (f) denoised image by MLTF; (g) denoised image by ISTF; (h) denoised image by STF; (i) denoised image by HTF.

multi-layer threshold function (MLTF) [30], improved symbolic threshold function (ISTF) [31], soft threshold function (STF) [24], hard threshold function (HTF) [24] and paper method (wavelet transform combined with improved PSO, WTPSO) are used for early CT image, advanced CT image and suspected cases of asymptomatic COVID-19 with different variance noise. Different Gaussian noise variance values ($\delta = 0.1, \delta = 0.2, \delta = 0.3, \delta = 0.4, \delta = 0.5, \delta = 0.6, \delta = 0.7$) are added to the image, and different decomposition levels n are selected at the same time. The experimental parameters are set as: $w_{max} = 0.9, w_{min} = 0.4, T_{max} = 150$. The particle population dimension is set as 5. The particle size is set as 50. When $\delta = 0.3, n = 3$, the denoised asymptomatic CT images of early COVID-19, advanced COVID-19 and suspected cases are shown in Figs. 4–7. From a visual point of view, the denoised image under WTPSO in this paper is clearer and the denoising effect is more obvious than the comparison methods.

In order to further verify the denoising effect of the improved threshold function in this paper on the objective data; Mean square error (MSE), peak signal-to-noise ratio (PSNR) and signal-to-noise ratio (SNR) and structural similarity (SSIM) are used to evaluate the denoised image. The lower the MSE, the better quality of the denoised image. The higher the PSNR and SNR, the better effect of the denoising method. SSIM is an index to measure the similarity of two different images. The range of SSIM is [0, 1], the value of SSIM is closer to 1, the more similar the two images are. It indicates that the effect of image denoising

method is better. The expression of MSE is:

$$MSE = \frac{1}{M \times N} \sum_{j=1}^M \sum_{l=1}^N [f(j, l) - \hat{f}(j, l)]^2 \quad (11)$$

The expression of PSNR is:

$$PSNR = 10 \times \lg \left(\frac{255^2}{MSE} \right) \quad (12)$$

The expression of SNR is:

$$SNR = 10 \lg \frac{\sum_{j=1}^M \sum_{l=1}^N f(j, l)^2}{\sum_{j=1}^M \sum_{l=1}^N [f(j, l) - \hat{f}(j, l)]^2} \quad (13)$$

The expression of SSIM is:

$$SSIM = \frac{(2 \times \mu_x \times \mu_y + c_1)(2 \times \sigma_{xy} + c_2)}{(\mu_x^2 + \mu_y^2 + c_1)(\sigma_x^2 + \sigma_y^2 + c_2)} \quad (14)$$

Where, μ_x and μ_y represent the average gray value of the original image and the denoised image respectively; σ_x^2 and σ_y^2 represent the grayscale

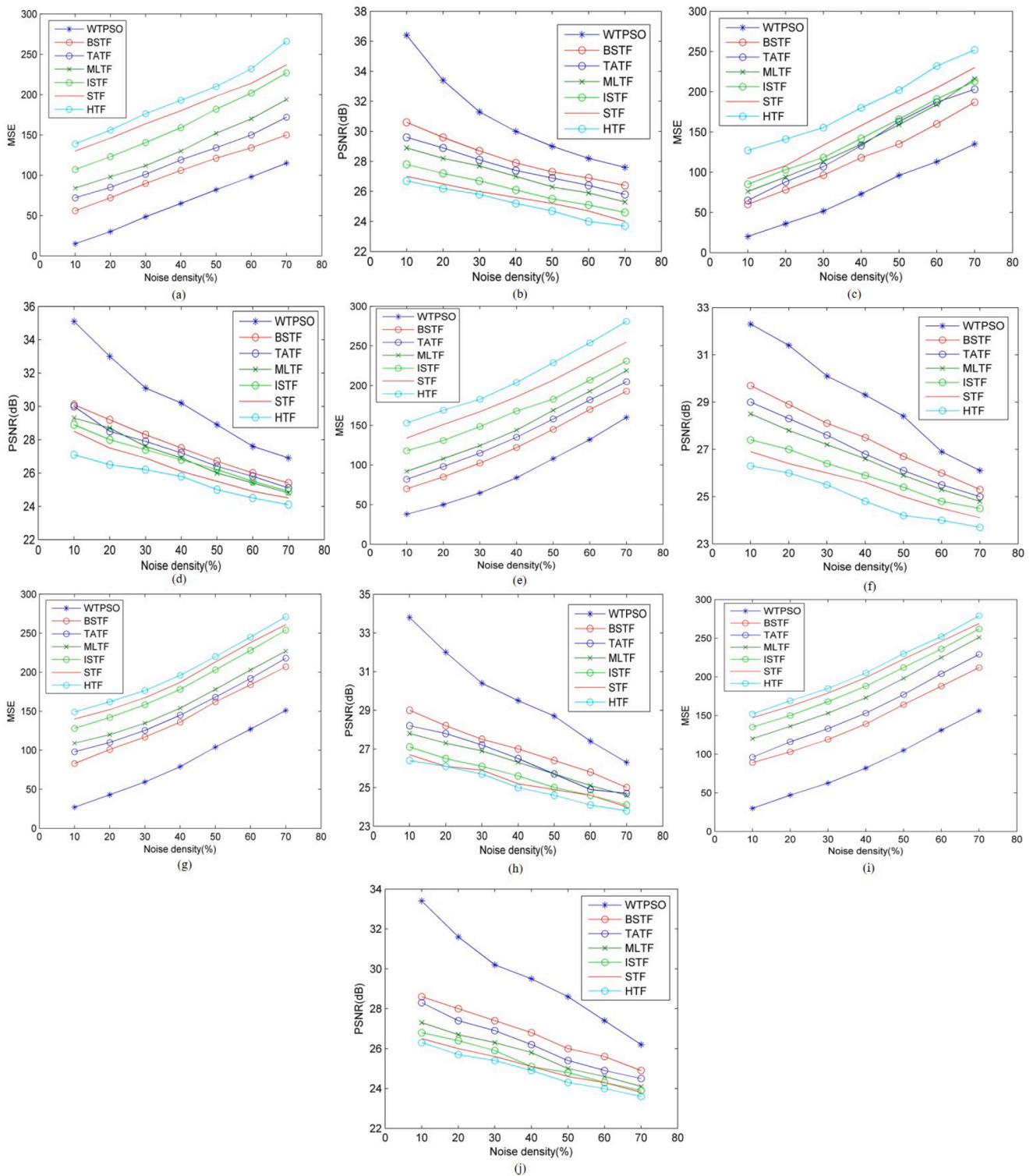


Fig. 7. Early asymptomatic COVID-19 with different noise density: (a) comparison of the MSE; (b) comparison of the PSNR. Advanced asymptomatic COVID-19 with different noise density: (c) comparison of the MSE; (d) comparison of the PSNR. Resolution asymptomatic COVID-19 with different noise density: (e) comparison of the MSE; (f) comparison of the PSNR. Influenza virus with different noise density: (g) comparison of the MSE; (h) comparison of the PSNR. Staphylococcal pneumonia with different noise density: (i) comparison of the MSE; (j) comparison of the PSNR.

variance value of the original image and the denoised image respectively; σ_{xy} represents the grayscale covariance of the original image and the denoised image; $c_1 = 6.4025, c_2 = 6.4025$. In the Equ.11–13, $f(j, l)$ represents the denoised signal, $\hat{f}(j, l)$ represents the input signal with Gaussian noise, M and N represent the length and width of the input

image; the picture size is 512 * 512. In order to compare the performance of the threshold function more comprehensively, different noise variances δ and different decomposition levels n are selected. The datas obtained through simulation are shown in Fig.7, 8.

Different threshold functions are tested on the noisy CT image of early asymptomatic COVID-19. The evaluation values are shown in

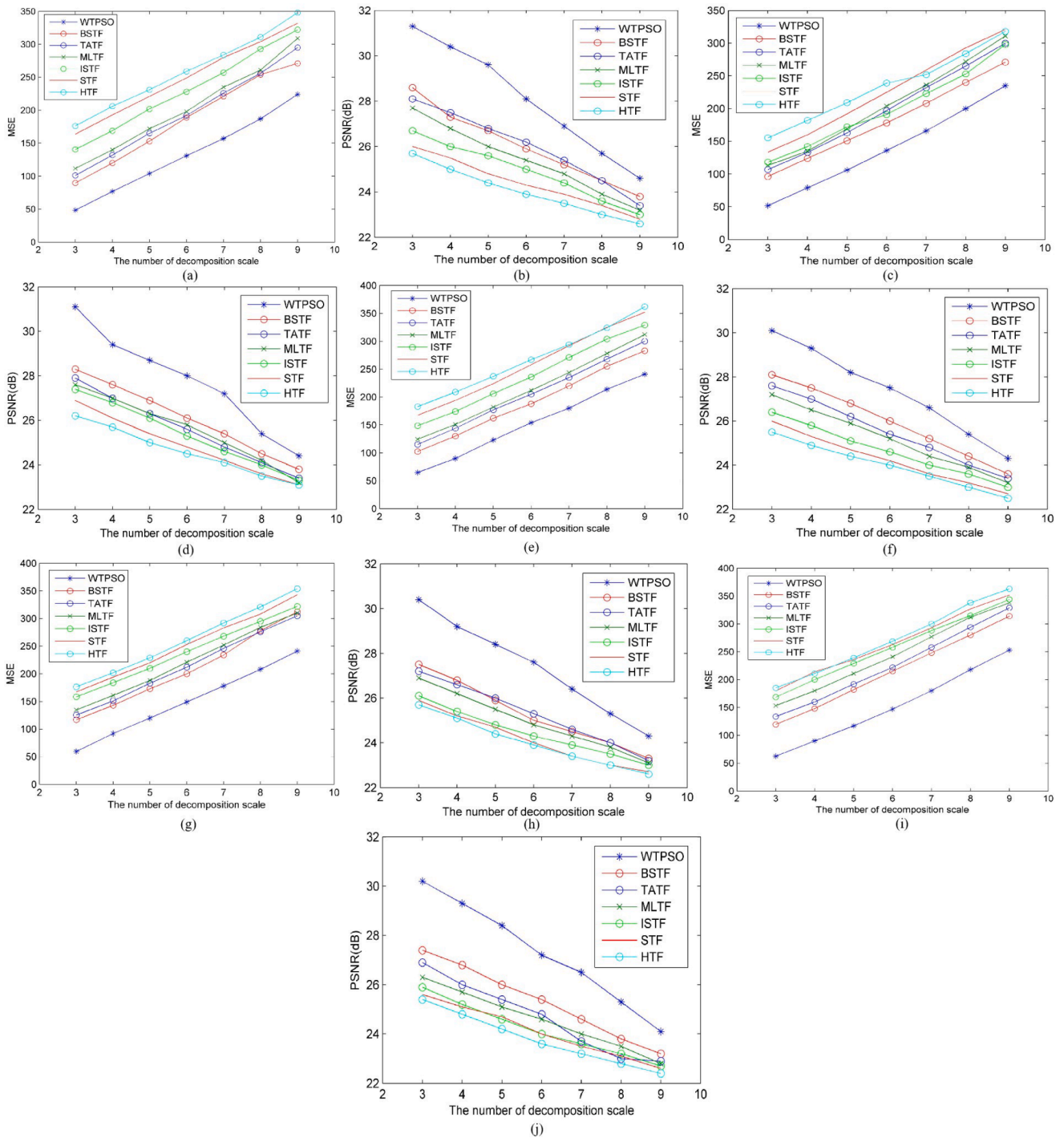


Fig. 8. Early asymptomatic COVID-19 with different decomposition scale: (a) comparison of the MSE; (b) comparison of the PSNR. Advanced asymptomatic COVID-19 with different decomposition scale: (c) comparison of the MSE; (d) comparison of the PSNR. Resolution asymptomatic COVID-19 with different decomposition scale: (e) comparison of the MSE; (f) comparison of the PSNR. Influenza virus with different decomposition scale: (g) comparison of the MSE; (h) comparison of the PSNR. Staphylococcal pneumonia with different decomposition scale: (i) comparison of the MSE; (j) comparison of the PSNR.

Table 1. From the change trend of the datas in the [Table 1](#), it can be seen that compared with the comparison methods, the PSNR under WTPSO has increased by about 5 dB, the MSE has been greatly reduced, and the SNR has increased by about 6.1 dB. The SSIM has increased by about 0.22. The maximum value of the PSNR under WTPSO is 31.3 dB, which is an increase of about 5.6 dB than the traditional hard threshold function. It can be seen that the denoising effect under WTPSO is the best. The traditional CT image denoising algorithms have the higher value of MSE and the lower value of PSNR. It is easy to cause the CT image to be

confused with noise, and it is easy to cause missed diagnosis for patients with early asymptomatic COVID-19. The WTPSO method improves the denoising accuracy for the CT image of early asymptomatic COVID-19. On the same way, different wavelet transform methods are tested on the noisy CT images of advanced asymptomatic COVID-19, resolution asymptomatic COVID-19 and suspected cases. The evaluation values of denoised images are shown in [Table 2-5](#).

From the change trend of the data in the [Table 2](#), compared with the comparative denoising methods, WTPSO has increased the value of

Table 1

Evaluation index of the denoising effect for early asymptomatic COVID-19 CT image ($n = 3, \delta=0.3$).

Denoising method	MSE	PSNR/dB	SNR/dB	SSIM
WTPSO	48.5	31.3	25.6	0.96
BSTF ^[4]	89.7	28.6	23.7	0.89
TATF ^[29]	101.2	28.1	22.4	0.84
MLTF ^[30]	111.8	27.7	21.7	0.81
ISTF ^[31]	140.5	26.7	21.2	0.77
STF ^[24]	163.8	26.0	20.5	0.75
HTF ^[24]	176.3	25.7	19.5	0.74

Table 2

Evaluation index of the denoising effect for advanced asymptomatic COVID-19 CT image ($n = 3, \delta=0.3$).

Denoising method	MSE	PSNR/dB	SNR/dB	SSIM
WTPSO	51.7	31.1	24.5	0.95
BSTF ^[4]	96.3	28.3	23.4	0.88
TATF ^[29]	106.9	27.9	21.9	0.86
MLTF ^[30]	113.3	27.6	21.3	0.80
ISTF ^[31]	118.1	27.4	20.7	0.76
STF ^[24]	133.6	26.9	19.6	0.73
HTF ^[24]	155.4	26.2	19.2	0.72

PSNR by about 3.5 dB, the value of MSE has been greatly reduced, the value of SNR has been increased by about 3.2 dB. The SSIM has increased by about 0.23. It can be seen that the denoising effect for the CT image of advanced asymptomatic COVID-19 under WTPSO is the best. In the advanced stage, asymptomatic COVID-19 lesions have been enlarged scope. The consolidation shadows can be seen inside the lesions, and the halo signs can be seen around them, which is easily misdiagnosed as suspected cases. The WTPSO method improves the denoising accuracy for the CT image of advanced asymptomatic COVID-19 and it reduces the misdiagnosis rate for the advanced lesions.

From the change trend of the data in the Table 3, compared with the comparative denoising methods, WTPSO has increased the value of PSNR by about 2.9 dB, the value of MSE has been greatly reduced, the value of SNR has been increased by about 4.3 dB. The SSIM has increased by about 0.24. It can be seen that the denoising effect for the CT image of resolution asymptomatic COVID-19 under WTPSO is the best. In the resolution stage, asymptomatic COVID-19 lesion has the narrow focus range and the smaller density, with a little thin ground-glass opacity, which is easy to be misdiagnosed as early COVID-19. The WTPSO method improves the denoising accuracy for the CT image of resolution asymptomatic COVID-19 and it reduces the misdiagnosis rate for the resolution lesions.

From the change trend of the data in the Table 4, compared with the comparative denoising methods, WTPSO has increased the value of PSNR by about 3.5 dB, the value of MSE has been greatly reduced, the value of SNR has been increased by about 5.3 dB. The SSIM has increased by about 0.23. It can be seen that the denoising effect for the CT image of influenza virus under WTPSO is the best. The lesion of influenza virus is generally distributed along the edge of the lung, with

Table 3

Evaluation index of the denoising effect for resolution asymptomatic COVID-19 CT image ($n = 3, \delta=0.3$).

Denoising method	MSE	PSNR/dB	SNR/dB	SSIM
WTPSO	64.7	30.1	25.6	0.94
BSTF ^[4]	102.4	28.1	22.8	0.86
TATF ^[29]	115.0	27.6	21.6	0.82
MLTF ^[30]	124.4	27.2	21.3	0.80
ISTF ^[31]	148.5	26.4	20.9	0.78
STF ^[24]	167.2	26.0	20.4	0.71
HTF ^[24]	182.8	25.5	19.6	0.70

patches or large blurred opacity, and it is easy to be misdiagnosed as advanced asymptomatic COVID-19. The WTPSO method improves the denoising accuracy for the CT image of influenza virus and it reduces the misdiagnosis rate for the asymptomatic COVID-19 suspected cases.

From the change trend of the data in the Table 5, compared with the comparative denoising methods, WTPSO has increased the value of PSNR by about 3.9 dB, the value of MSE has been greatly reduced, the value of SNR has been increased by about 4.5 dB. The SSIM has increased by about 0.24. It can be seen that the denoising effect for the CT image of staphylococcal pneumonia under WTPSO is the best. The staphylococcal pneumonia presents a single diffuse ground-glass opacity with unclear boundary, which can be accompanied by consolidation opacity and bronchial wall thickening. It is easy to be misdiagnosed as resolution asymptomatic COVID-19. The WTPSO method improves the denoising accuracy for the CT image of staphylococcal pneumonia and it reduces the misdiagnosis rate for the asymptomatic COVID-19 suspected cases.

For the noisy CT image of early asymptomatic COVID-19, the number of wavelet decomposition layers is 3, and different noise variances are set up. The value of PSNR changes with the variance of noise. The simulation results is shown in Fig.7(b). It can be seen from the trend of the curve that the PSNR decreases gradually with the increase of noise variance. Compared with the PSNR under other comparison functions, the PSNR under the paper method is still the largest and the denoising effect is ideal. The value of MSE increases with the increase of noise variance. The simulation results is shown in Fig.7(a). It can be seen from the trend of the curve that when the noise variance increases, the MSE under the six comparison functions increases. When the variance increases to 0.8, the MSE under the paper method is higher than the other comparison methods. On the same way, different threshold denoising methods are used on the CT images of the advanced asymptomatic COVID-19, resolution asymptomatic COVID-19 and the suspected cases. The simulation results are shown in Fig.7(c)-(j).

For the CT image of early asymptomatic COVID-19, the noise variance is set to 0.3, and different wavelet decomposition levels are set. The value of PSNR changes with the change of the decomposition levels. The simulation results are shown in Fig.8(b). From the change trend of the curve, it can be seen that the value of PSNR is different with the number of wavelet decomposition layers. With the increase of the number of wavelet decomposition layers, the PSNR shows a downward trend, and the useful information in the noisy image will be lost. The noise variance is taken as 0.3 and setting different wavelet decomposition levels n , the

Table 4

Evaluation index of the denoising effect for influenza virus CT image ($n = 3, \delta=0.3$).

Denoising method	MSE	PSNR/dB	SNR/dB	SSIM
WTPSO	59.4	30.4	25.8	0.94
BSTF ^[4]	116.9	27.5	21.7	0.87
TATF ^[29]	125.4	27.2	21.2	0.85
MLTF ^[30]	134.7	26.9	20.5	0.81
ISTF ^[31]	158.4	26.1	19.8	0.80
STF ^[24]	167.3	25.9	19.4	0.72
HTF ^[24]	176.5	25.7	18.3	0.71

Table 5

Evaluation index of the denoising effect for staphylococcal pneumonia CT image ($n = 3, \delta=0.3$).

Denoising method	MSE	PSNR/dB	SNR/dB	SSIM
WTPSO	62.5	30.2	24.7	0.94
BSTF ^[4]	119.6	27.4	21.4	0.86
TATF ^[29]	133.7	26.9	20.8	0.84
MLTF ^[30]	153.3	26.3	20.2	0.80
ISTF ^[31]	168.5	25.9	19.6	0.77
STF ^[24]	179.8	25.6	19.1	0.72
HTF ^[24]	185.3	25.4	18.5	0.70

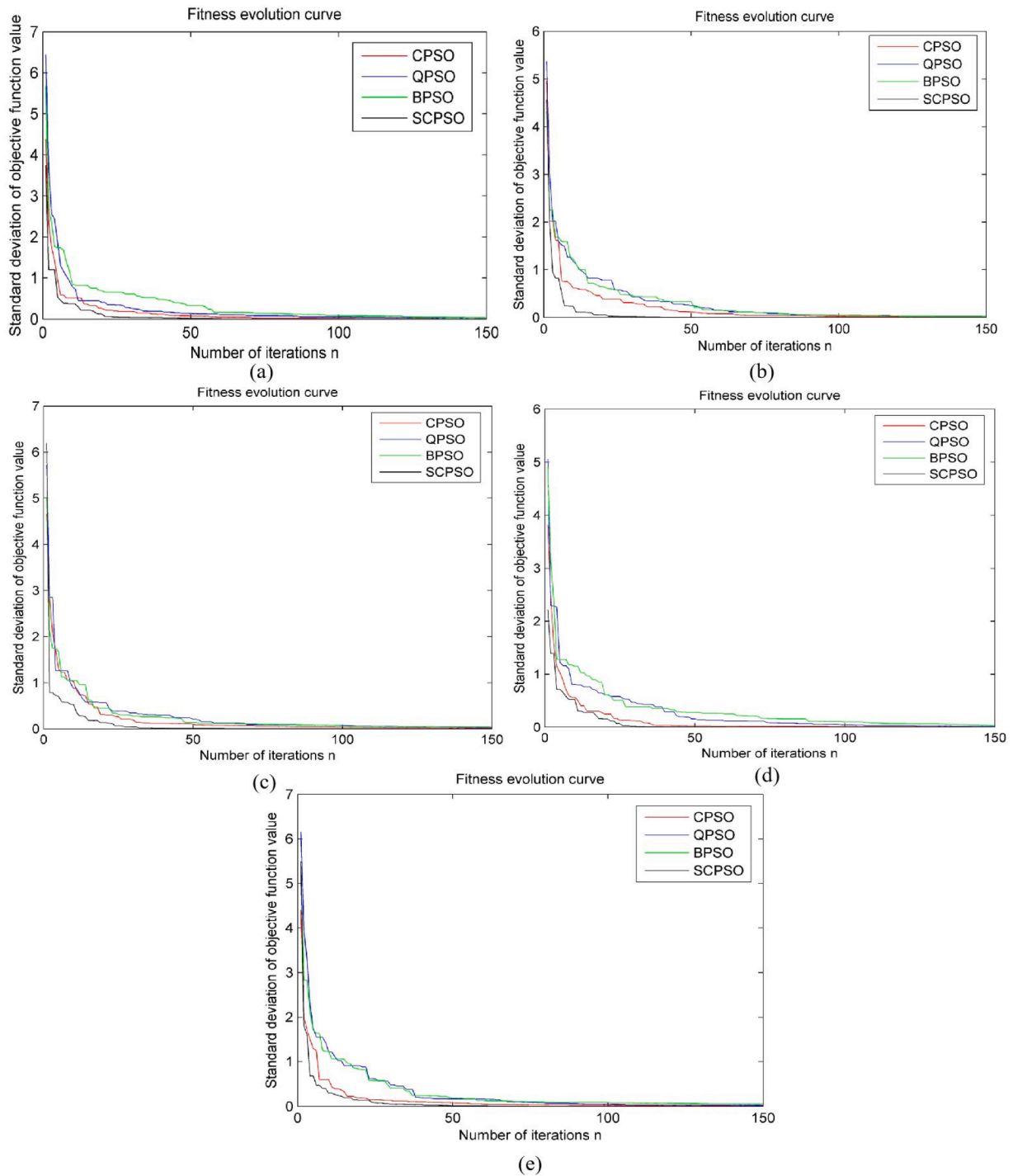


Fig. 9. Fitness evolution curve of denoising parameters optimization for different CT images. (a) Early asymptomatic COVID-19; (b) Advanced asymptomatic COVID-19; (c) Resolution asymptomatic COVID-19; (d) Influenza virus; (e) Staphylococcal pneumonia.

MSE is also different. Taking the noise variance as 0.3 and setting different times of wavelet decomposition layer, the value of MSE is also different. The simulation results are shown in Fig.8(a). According to the change trend of the curve, the MSE shows an upward trend with the increase of the number of wavelet decomposition layers. When the same number of wavelet decomposition layer is taken, the MSE under the paper method is greater than the other comparison methods, indicating that the effect of the paper method is ideal. Similarly, the CT images of advanced asymptomatic COVID-19 and suspected cases are tested by different threshold denoising methods among different decomposition levels. The simulation results are shown in Fig.8(c)-(j). From the analysis

of the above simulation experimental data, it can be seen that the PSNR decreases with the increase of the noise variance. The MSE rises with the increase of the noise variance. Compared with the other comparison methods, the WTPSO in this paper improves the PSNR to a certain extent. It reduces the MSE and significantly improves the denoising effect.

Aiming at the different kinds of asymptomatic COVID-19 CT images, competitive particle swarm optimization (CPSO) [32], quantum particle swarm optimization (QPSO) [33], binary particle swarm optimization (BPSO) [34], sine/cosine adjusted particle swarm optimization (SCPSO, paper method) are used for simulation of denoising parameters

Table 6
Time processing of CT image denoised under different methods

CT image	CPSO ^[32]	QPSO ^[33]	BPSO ^[34]	SCPSO
Early asymptomatic COVID-19	3.56	3.72	3.77	2.87
Advanced asymptomatic COVID-19	3.92	4.08	4.14	2.68
Resolution asymptomatic COVID-19	3.84	3.98	4.05	3.15
Influenza virus	3.33	4.08	4.14	3.06
Staphylococcal pneumonia	3.36	3.94	4.11	3.14

optimization. The fitness evolution curve for different asymptomatic COVID-19 CT images are shown in Fig.9. The evaluation index values of time processing under different methods are shown in Table 6.

It can be seen from the Fig.9 and Table 6 that with the increase of the number of iterations, the standard deviation of the objective function is gradually reduced and the processing time is gradually increased under different parameters optimization methods. Compared with the different comparison methods, the number of iterations of SCPSO is still the smallest, and the processing time of SCPSO is still the fastest. In conclusion, the paper method (SCPSO) significantly improves the denoised effect for different kinds of COVID-19 CT images of parameters optimization with relatively few iterations. From the change trend of the data in the Table 6 and Fig.9, compared with the comparative PSO optimization methods for the early asymptomatic COVID-19, SCPSO has decreased the value of running time by about 0.8s, and the number of iterations is reduced by about 40. It can be seen that the average computational time complexity for the CT image of early asymptomatic COVID-19 under SCPSO is the lowest. Therefore, it can be concluded that under the premise of obtaining the same optimal value, the average computational time complexity of the improved PSO is reduced by at least 25% compared to the comparison PSO methods.

5. Conclusion

In this paper, the CT image denoising method for asymptomatic COVID-19 based on wavelet transform combined with improved PSO is proposed. By selecting different noise variance and different wavelet decomposition layer, the three evaluation indexes are compared and analyzed under the comparison methods and paper method. In this paper, the wavelet threshold adopts the shrinkage factor. Therefore, different threshold values can be calculated for different decomposition layers, which increases the flexibility for threshold selection. It reduces the missed diagnosis for early and resolution asymptomatic COVID-19. At the same time, the wavelet threshold function includes adjustment factor integrated with the arc tangent. The optimal wavelet estimation coefficient is obtained by changing the adjustment parameters based on the improved PSO. It reduces the mistake diagnosis for advanced asymptomatic COVID-19 with suspected cases. The simulation results show that the denoising effect based on the paper method is more ideal than other denoising methods. Although the improved wavelet transform proposed in this paper has a good denoising effect on Gaussian noise, there are many types of noise on CT image. Whether the denoising effect of other types of noise is ideal still needs in-depth research and experiments.

CRedit authorship contribution statement

Guowei Wang: Writing - original draft, Methodology, Software. **Shuli Guo:** Conceptualization, Data curation. **Lina Han:** Writing - review & editing. **Anil Baris Cekderi:** Visualization. **Xiaowei Song:** Investigation. **Zhilei Zhao:** Validation.

Declaration of Competing Interest

The authors declare that they have no known competing financial interests or personal relationships that could have appeared to influence the work reported in this paper.

Acknowledgements

This research has been partially funded by National Key R&D Program of China(2017YFF0207400) and project supported by Beijing Municipal Science and Technology Commission-Beijing Natural Science Foundation(M21018) and Beijing Natural Science Foundation-haidian District Joint Fund for original innovation(L192064).

References

- [1] Isaac Kyei-Barfour, Samuel Akwetey Addo, Enoch Aninagyei, George Ghartey-Kwansah, and Desmond Omame Acheampong. Sterilizing immunity against covid-19: Developing helper t cells i and ii activating vaccines is imperative, *Biomed. Pharmacother.*, 144:112282–112282, 2021.
- [2] Emin Uysal, Abidin Kılınċer, Hakan Cebeci, Halil Özer, Nazlım Aktuğ Demir, Mehmet Öztürk, Mustafa Koplay, Chest ct findings in rt-pcr positive asymptomatic covid-19 patients, *Clin. Imaging* 77 (2021) 37–42.
- [3] Yun Shan Goh, Jean-Marc Chavatte, Alicia Lim Jieling, Bernett Lee, Pei Xiang Hor, Siti Naqiah Amrun, Cheryl Yi-Pin Lee, Rhonda Sin-Ling Chee, Bei Wang, Chia Yin Lee, Eve Zi Xian Ngoh, Cheng-I Wang, Barnaby Edward Young, Paul Anantharajah Tambyah, Shirin Kalimuddin, Surinder M.S. Kaur Pada, Seow Yen Tan, Louisa Jin Sun, Mark I-Cheng Chen, Yee Sin Leo, David Chien Boon Lye, Lisa F.P. Ng, Raymond Tzer Pin Lin, and Laurent Réna. Sensitive detection of total anti-spike antibodies and isotype switching in asymptomatic and symptomatic individuals with covid-19. *Cell Reports Medicine*, 2, 2021.
- [4] Mamta Juneja, Sumindar Kaur Saini, Sambhav Kaul, Rajarshi Acharjee, Niharika Thakur, Prashant Jindal. Denoising of magnetic resonance imaging using bayes shrinkage based fused wavelet transform and autoencoder based deep learning approach, *Biomed. Signal Process. Control.* 69 (2021), 102844.
- [5] Xin Dong, Guolong Li, Yachao Jia, Biao Li, Kun He, Non-iterative denoising algorithm for mechanical vibration signal using spectral graph wavelet transform and detrended fluctuation analysis, *Mech. Syst. Signal Process.* 149 (2021), 107202.
- [6] Hari Mohan Rai, Kalyan Chatterjee, Hybrid adaptive algorithm based on wavelet transform and independent component analysis for denoising of mri images, *Measurement* (2019).
- [7] Hilal Naimi, Amel B.H. Adamou-Mitiche, Lahcène Mitiche, Medical image denoising using dual tree complex thresholding wavelet transform and wiener filter. *J. King Saud Univ. Comput. Inf. Sci.* 27 (2015) 40–45.
- [8] S. Shruithi, K.G. Satheshkumar, Constrained least squares filtering followed by denoising of decomposed images using wave atom and wavelet transform, *Procedia Comput. Sci.* 115 (2017) 526–532.
- [9] Hu. Kai, Qiaocui Cheng, Bodong Li, Xieping Gao, The complex data denoising in mr images based on the directional extension for the undecimated wavelet transform, *Biomed. Signal Process. Control.* 39 (2018) 336–350.
- [10] Dongming Li, Lijuan Zhang, Jinhua Yang, Su. Wei, Research on wavelet-based contourlet transform algorithm for adaptive optics image denoising, *Optik* 127 (2016) 5029–5034.
- [11] S.K. Prateep Upadhyay, Upadhyay, and Kaushal Kumar Shukla. Magnetic resonance images denoising using a wavelet solution to laplace equation associated with a new variational model, *Appl. Math. Comput.* 400 (2021), 126083.
- [12] Simi Venuji Renuka, Damodar Reddy Edla, Adaptive shrinkage on dual-tree complex wavelet transform for denoising real-time mr images, *Biocybern. Biomed. Eng.*, 2019.
- [13] Khuram Naveed, Muhammad Tahir Akhtar, Muhammad Faisal Siddiqui, Naveed ur Rehman, A statistical approach to signal denoising based on data-driven multiscale representation, *Digit. Signal Process.* 108 (2021), 102896.
- [14] Shohidul Islam, Yuanyuan Zhu, Imran Hossain, Rizwan Ullah, Zhongfu Ye, Supervised single channel dual domains speech enhancement using sparse non-negative matrix factorization, *Digit. Signal Process.* 100 (2020), 102697.
- [15] Huan Luo, Miaohua Huang, Zhou Zhou, A dual-tree complex wavelet enhanced convolutional lstm neural network for structural health monitoring of automotive suspension, *Measurement* (2019).
- [16] Navdeep Prashar, Meenakshi Sood, Shruti Jain, Design and implementation of a robust noise removal system in eeg signals using dual-tree complex wavelet transform, *Biomed. Signal Process. Control.* 63 (2021), 102212.
- [17] A.H. Lenin, S.M. Vasanthi, T. Jayasree, Automated recognition of hand grasps using electromyography signal based on lwt and dtcwt of wavelet energy, *Int. J. Comput. Intell. Syst.* 13 (1) (2020).
- [18] D. Li, L. Zhang, C. Sun, T. Yin, C. Liu, J. Yang, Robust retinal image enhancement via dual-tree complex wavelet transform and morphology-based method, *IEEE Access* 7 (2019) 47303–47316.
- [19] Siyuan Wang, Junjie Lv, Hu. Yuanyuan, Dong Liang, Minghui Zhang, Qiegen Liu, Denoising auto-encoding priors in undecimated wavelet domain for mr image reconstruction, *Neurocomputing* 437 (2021) 325–338.

- [20] Chandan Singh, Sukhjeet K. Ranade, Karamjeet Singh, Invariant moments and transform-based unbiased nonlocal means for denoising of mr images, *Biomed. Signal Process. Control.* 30 (2016) 13–24.
- [21] Chan-Cheng Liu, Tsung-Ying Sun, Shang-Jeng Tsai, Yu. Yu-Hsiang, Sheng-Ta Hsieh, Heuristic wavelet shrinkage for denoising, *Appl. Soft Comput.* 11 (2011) 256–264.
- [22] Xiang yu Zhong, Xuanhua Xu, Bin Pan, A non-threshold consensus model based on the minimum cost and maximum consensus-increasing for multi-attribue large group decision-making, *Inf. Fusion* 77 (2022) 90–106.
- [23] Bo Xie, Zhangqiang Xiong, Zhijian Wang, Lijiao Zhang, Dazhou Zhang, Fusheng Li, Gamma spectrum denoising method based on improved wavelet threshold, *Nucl. Eng. Technol.* 52 (2020) 1771–1776.
- [24] Rui Zhao, Hui-Min Cui, Improved threshold denoising method based on wavelet transform, in: 2015 7th International Conference on Modelling, Identification and Control (ICMIC), 2015, pp. 1–4.
- [25] Wei Zhu, Hima Nikafshan Rad, Mahdi Hasanipanah, A chaos recurrent anfis optimized by pso to predict ground vibration generated in rock blasting, *Appl. Soft Comput.* 108 (2021), 107434.
- [26] Hao Feng, Wei Ma, Chenbo Yin, Donghui Cao, Trajectory control of electro-hydraulic position servo system using improved pso-pid controller, *Automat. Constr.* (2021).
- [27] S. Thomas George, M.S.P. Subathra, N.J. Sairamya, L. Susmitha, M. Joel Premkumar, Classification of epileptic eeg signals using pso based artificial neural network and tunable-q wavelet transform, *Biocybern. Biomed. Eng.* 40 (2020) 709–728.
- [28] Wuge Chen, Junning Li, Qian Wang, Ka. Han, Fault feature extraction and diagnosis of rolling bearings based on wavelet thresholding denoising with ceemdan energy entropy and pso-lssvm, *Measurement* 172 (2021), 108901.
- [29] Tahsina Farah Sanam, Celia Shahnaz, Noisy speech enhancement based on an adaptive threshold and a modified hard thresholding function in wavelet packet domain, *Digit. Signal Process.* 23 (2013) 941–951.
- [30] Weibiao Qiao, Mohammad Khishe, Sajjad Ravakhah, Underwater targets classification using local wavelet acoustic pattern and multi-layer perceptron neural network optimized by modified whale optimization algorithm, *Ocean Eng.* 219 (2021), 108415.
- [31] Dominik P. Storhas, Lurion De Mello, Abhay K. Singh, Multiscale lead-lag relationships in oil and refined product return dynamics: A symbolic wavelet transfer entropy approach, *Energy Economics* 92 (2020), 104927.
- [32] Keurfon Luu, Mark Noble, Alexandrine Gesret, Nidhal Belayouni, Pierre-François Roux, A parallel competitive particle swarm optimization for non-linear first arrival traveltime tomography and uncertainty quantification, *Comput. Geosci.* 113 (2018) 81–93.
- [33] Quanyuan Zhang, Haolun Li, Yanli Liu, Shangrong Ouyang, Caiting Fang, Mu. Wentao, Hao Gao, A new quantum particle swarm optimization algorithm for controller placement problem in software-defined networking, *Comput. Electr. Eng.* 95 (2021), 107456.
- [34] An-Da Li, Bing Xue, Mengjie Zhang, Improved binary particle swarm optimization for feature selection with new initialization and search space reduction strategies, *Appl. Soft Comput.* 106 (2021), 107302.